Wave power assessment in Faroese waters using an oceanic to nearshore scale spectral wave model

Joensen, Bárður; Niclasen, Bárður A.; Bingham, Harry B.

Published in:
Energy

Link to article, DOI:
10.1016/j.energy.2021.121404

Publication date:
2021

Document Version
Publisher's PDF, also known as Version of record

Energy 235 (2021) 121404

Contents lists available at ScienceDirect

Energy

journal homepage: www.elsevier.com/locate/energy

Wave power assessment in Faroese waters using an oceanic to nearshore scale spectral wave model

Bárður Joensen [a, b, *], Bárður A. Niclasen [c], Harry B. Bingham [b]

[a] LBF Consulting Engineers, Niels Finsensgøta 10, FO-110 Tórshavn, Faroe Islands
[b] Technical University of Denmark, Department of Mechanical Engineering, Section for Fluid Mechanics, Coastal and Maritime Engineering, Nils Koppels Allé building 404, 2800, Kgs. Lyngby, Denmark
[c] University of Faroe Islands, Department of Science & Technology, Vestara Bryggja 15, FO-100 Tórshavn, Faroe Islands

ARTICLE INFO

Article history:
Received 2 January 2021
Received in revised form
8 May 2021
Accepted 1 July 2021
Available online 8 July 2021

Keywords:
Wave power
Spectral wave model
MIKE 21 SW
Wave hindcasting
Faroe Islands

ABSTRACT

It is expected that wave power will first become an economically competitive energy source in isolated electrical grids located in exposed regions. One such candidate is the Faroe Islands. The goal of this paper is to map the local wave power potential around the Faroe Islands using the spectral wave model MIKE 21 SW. A model is set up for the entire North Atlantic Ocean. The model is forced by 10 years of ERA5 reanalysis wind data and is validated against several directional offshore wave buoys along with nearshore acoustic Doppler current profile measurements. The results show that the wave climate is dominated by waves from south-to-west and to a lesser extent from northerly directions, while waves from other directions are more moderate and infrequent. The average wave energy flux at nearshore locations to the west and north is 45–55 kW/m, while significantly lower flux of 10–25 kW/m is found at eastern locations. The results show that the maximum significant wave heights are 12–14 m to the west, 9–13 m to the north and 8–9 m to the east. This energy assessment will provide the basis for an evaluation of wave energy absorption concepts suitable for deployment in the Faroese waters.

1. Introduction

Due to a heavy dependence on fossil fuels and the threatening side effects of greenhouse gasses, governments are called upon to take action, and significantly increase energy production from renewable energy sources. The Faroese government, together with the local electricity company (SEV), have announced that they aim to achieve 100% carbon emissions-free land-based energy production by 2030. In recent years the local share of renewable production has been 40% from hydro- and wind-power, with 60% coming from oil. The relatively high dependence on imported oil makes the electricity price, among the highest in the world [1]. The high cost of production is a hidden asset in the transformation towards a 100% renewable energy system, as projects based on renewable sources can have a lower price of energy relative to existing oil based production. Recent developments and plans for variable renewable production, aided by pumped storage systems support the realization of renewable land-based energy production [2,3], but with restrictions for further development of hydro-power,

* Corresponding author. Technical University of Denmark, Department of Mechanical Engineering, Section for Fluid Mechanics, Coastal and Maritime Engineering, Nils Koppels Allé building 404, 2800, Kgs. Lyngby, Denmark.
E-mail address: bajoe@mek.dtu.dk (B. Joensen).

https://doi.org/10.1016/j.energy.2021.121404
0360-5442/

there could be a need for additional alternatives to wind and solar power to achieve 100% production from renewable sources [4].

ρ	Density of water [kg/m^3]
σ	Intrinsic angular frequency [rad/s]
$c(\sigma, \theta)$	Propagation velocity in spectral space
c_x	Propagation velocity in x-direction [m/s]
c_y	Propagation velocity in y-direction [m/s]
Dir_p	Peak wave direction [deg]
$E(\sigma, \theta)$	Wave energy spectrum [m^2 s/rad]
g	Gravitational acceleration [m/s^2
h	Water depth [m]
H_{m0}	Significant wave height [m]
k_e	Wave number based on energy period [m^{-1}]
N	Wave action density
P	Wave energy flux [kW/m]
P_{annual}	Annual mean wave energy [MWh/m]
p_{hourly}	Hourly occurrence of sea state [−]
S_{bot}	Bottom friction dissipation
S_{ds}	White-capping dissipation
S_{in}	Momentum transfer of wind to wave generation
S_{nl}	Nonlinear wave-wave interaction
S_{surf}	Depth-induced wave breaking
S_{tot}	Total source term
t	Time variable [s]
T_e	Energy period [s]
T_p	Peak wave period [s]
θ	Wave direction [rad]
ADCP	Acoustic Doppler Current Profiler
CDS	Climate Data Store
DIA	Discrete Interaction Approximation
ECMWF	European Center for Medium Range Weather Forecast
ERA5	5th generation ECMWF reanalysis dataset for global climate and weather
GEBCO	General Bathymetric Chart of the Oceans
HIRLAM	High Resolution Limited Area Modeling
MIKE 21 NSW	DHI's Near-shore spectral wind-wave model (no longer available)
MIKE 21 SW	DHI's 3rd generation spectral wave model
NCAR	National Center for Atmospheric Research
NCEP	National Centers for Environmental Prediction
PNJ	Pierson-Neumann-James wave prediction method
R	Correlation coefficient
RMSE	Root-mean-square error
SI	Scatter index
SMB	Sverdrup-Munk-Bretschneider wave prediction method
SWAN	3rd generation spectral wave model developed by Delft University
WAM	3rd generation ocean wave prediction model
WaveWatch III	3rd generation ocean wave model

Recent developments in wave power production look both interesting and promising. Furthermore, there is a lot of investment in research and development of wave energy conversion concepts/techniques [5]. A lot of work has been performed to assess the potential for wave power production worldwide. This generally involves running numerical spectral wave model hindcasts, which are validated against measured data. Locations such as Northeast Asia [6], Sri Lanka [7] and the South China Sea [8] have been studied. For the aforementioned studies, SWAN [9] was used to develop the wave model, and was forced using wind data from the Japan Meteorological Agency [10]. Furthermore, many studies have been performed that analyze the coasts of North America in terms of wave energy assessment [11–14]. Refs. [12–14] used WaveWatch III [15], while [11] ran nested simulations in WaveWatch III and used SWAN to run high resolution simulations for the nearshore climate. With a more global perspective [16], compiled an atlas of the global wave energy resource, using WaveWatch III. This showed that the North Atlantic Ocean, specifically the Northeast Atlantic Ocean, holds high amounts of wave energy. The Bay of Biscay and the Iberian Peninsula are locations which have been studied extensively for wave energy potential assessment. Ref. [17] developed a wave model using SWAN and forced at the offshore boundary using wave measurement buoys. Refs. [18] and [19] both used WAM [20], while [18] used global atmospheric data from (NCEP) and (NCAR) [19,21] used the HIRLAM [22] numerical model for atmospheric data. Refs. [23,24], and [25] developed an offshore model using WAM, and ran nested simulations to feed in to a coastal SWAN model, while [26] only used SWAN to develop their model. Furthermore, Scottish waters have also been an area under consideration [27]. This study used MIKE 21 SW [28], a sub model in DHI's MIKE 21 model suite, and forced the model using wind data from ECMWF [29].

There exist several studies on the wave power potential in island communities in the North Atlantic Ocean e.g. Refs. [30–34], but

none on the high resolution mapping of the wave energy potential on the Faroe Shelf. A few local studies have been conducted to analyze wave conditions around the islands. Ref. [35] used analytical methods, such as the SMB method (Sverdrup-Munk-Bretschneider) [36], Wilson's method [36] and the PNJ method (Pierson-Neumann-James) [37]. Ref. [38] used MIKE 21 NSW (Near-shore spectral wind-wave model) forced by local wave buoy measurements to analyze the wave climate around the islands. Also short time hindcasts from an operational wave model [39] using SWAN, forced by wind have been used to estimate the wave climate. However, none of these have focused on mapping the wave energy potential, although some introductory estimates have been derived based on local measurements [40]. The previous local studies on the wave climate around the Faroe Islands, have shown that there are large wave heights present. The western and northern coasts are dominated by larger wave heights, compared to the eastern coasts. Ref. [41] showed values of an estimated 10-year maximum significant wave height of 16 m at the western and northern coasts. However, none of the previous studies show any details on the wave periods, and the information on the wave energy is very limited.

By taking advantage of faster computers and the ability to run a wave model with an unstructured mesh, which is coarse offshore but with high resolution nearshore, it is now for the first time feasible to map the local wave power potential with high resolution for the waters surrounding the Faroe Islands, without any simplifying assumptions on the forcing, wave field or wave model physics. Compared to other local studies, this investigation is also validated against more data and over a longer time-span.

The objective of the present work is to evaluate and assess the wave climate around the Faroe Islands. This is done by using wave buoy measurements and numerical wave modelling. The numerical wave model used in this study is MIKE 21 SW. The area around the Faroe Islands holds a vast amount of wave energy, making it a viable candidate for wave energy conversion. Wave energy content is high but this is also a challenge, as the Faroe Islands are located close to one of the harshest recorded wave climates in the world [42]. This is challenging, due to the potentially large forces associated with large and steep waves making the design of the proposed wave energy devices more expensive.

2. Model overview

When modeling waves at scales where instationary wave growth is important, the standard approach is to use spectrally averaged wave models. These models predict the growth, transformation and decay of ocean waves, due to their interaction with ocean surface winds and bathymetry. In the present study, such a spectral wave model is used. The underlying concept of spectral wave models is the energy balance equation, where the evolution of the wave spectrum is given by:

$$\frac{\partial E}{\partial t}+\frac{\partial}{\partial x}(c_x E)+\frac{\partial}{\partial y}(c_y E)+\frac{\partial}{\partial \sigma}(c_\sigma E)+\frac{\partial}{\partial \theta}(c_\theta E)=S_{tot} \quad (1)$$

where $E(\sigma, \theta)$ is the wave energy spectrum, t is time, σ is the intrinsic angular frequency, θ is the wave direction, c_x and c_y are the propagation velocities in the geographical space, while c_σ and c_θ are the propagation velocities in the spectral space. The first term represents the local rate of change of energy density in time. The second and third terms represent the geographic propagation of energy density in the (x,y)-space. The fourth term represents the shifting of the frequency due to depth variations, and the fifth and last term is related to depth-induced refraction with propagation velocity c_θ in the θ-space. In short, the left hand side of Equation (1) constitutes the propagation of a large sum of independent linear waves.

The right hand side of Equation (1) represents the effects of generation, dissipation and nonlinear wave-wave interaction. The total source term is expressed as

$$S_{tot}=S_{in}+S_{nl}+S_{ds}+S_{bot}+S_{surf} \quad (2)$$

where S_{in} is the momentum transfer of wind energy to wave generation, S_{nl} is the nonlinear wave-wave interaction (triad and quadruplet), S_{ds} is the dissipation of energy due to white-capping, S_{bot} is the dissipation of energy due to bottom friction and S_{surf} is the dissipation of energy due to depth-induced wave breaking. In deep water the evolution of the spectrum is dominated by the balance between S_{in}, S_{ds} and the quadruplet part of S_{nl}. In shallower water the triad part of S_{nl}, S_{bot} as well as S_{surf} become increasingly important parts of the evolution. The input term S_{in} works at all depth ranges, increasing the amplitudes of wave components traveling in a similar direction to the wind, but with lower phase speeds.

For this particular study the third-generation spectral wave model MIKE 21 SW has been used for modeling the waves [43]. This model discretizes the governing equations in geographical and spectral space using a cell-centered finite volume method. In the geographical domain an unstructured mesh technique is used. The time integration is performed using a fractional step approach where a multi-sequence explicit method is applied for the propagation of wave action [28].

The source functions S_{in}, S_{nl}, and S_{ds} are similar to those in the WAM Cycle 4 model [44]. The wind input is based on Janssen's ([45,46]) quasi-linear theory of wind-wave generation, where the momentum transfer from the wind to the sea not only depends on the wind stress, but also on the sea-state. The quadruplet wave-wave interaction is based on the computationally efficient Discrete Interaction Approximation (DIA) proposed in Ref. [47] and the S_{ds} term is based on the formulation of white-capping in Ref. [44].

There is also the possibility of including variations due to wave-current interactions and time-varying water depth, in which the wave action density N becomes the dependent parameter. Since no wave-current interactions and time-varying water depth are considered in this study, this will not be described here.

3. Model set-up

This section provides details on how the model has been set up. Bathymetry, mesh, model forcing and physical processes will be reviewed here.

3.1. Bathymetry and mesh

As mentioned previously, the study area is the waters around the Faroe Islands. Fig. 1 shows the oceanic scale computational domain (left), together with the refined grid around the Faroe Islands (right). An unstructured computational mesh has been used for the computational domain. This is constructed using the MIKE mesh-generator, and it covers the area 70°W to 10°E and 5°N to 80°N. Swells generated in the Atlantic Ocean travel long distances and reach the Faroe Islands with little loss of wave energy. This is a positive feature for the extraction of energy from waves. In order to catch all the swells traveling from the Atlantic, it was necessary to use a large computational model, even though, the area of interest is mainly around the Faroe Islands. Bathymetry data was acquired from the General Bathymetric Chart of the Oceans (GEBCO) [48], and these were used to generate the mesh for the model domain.

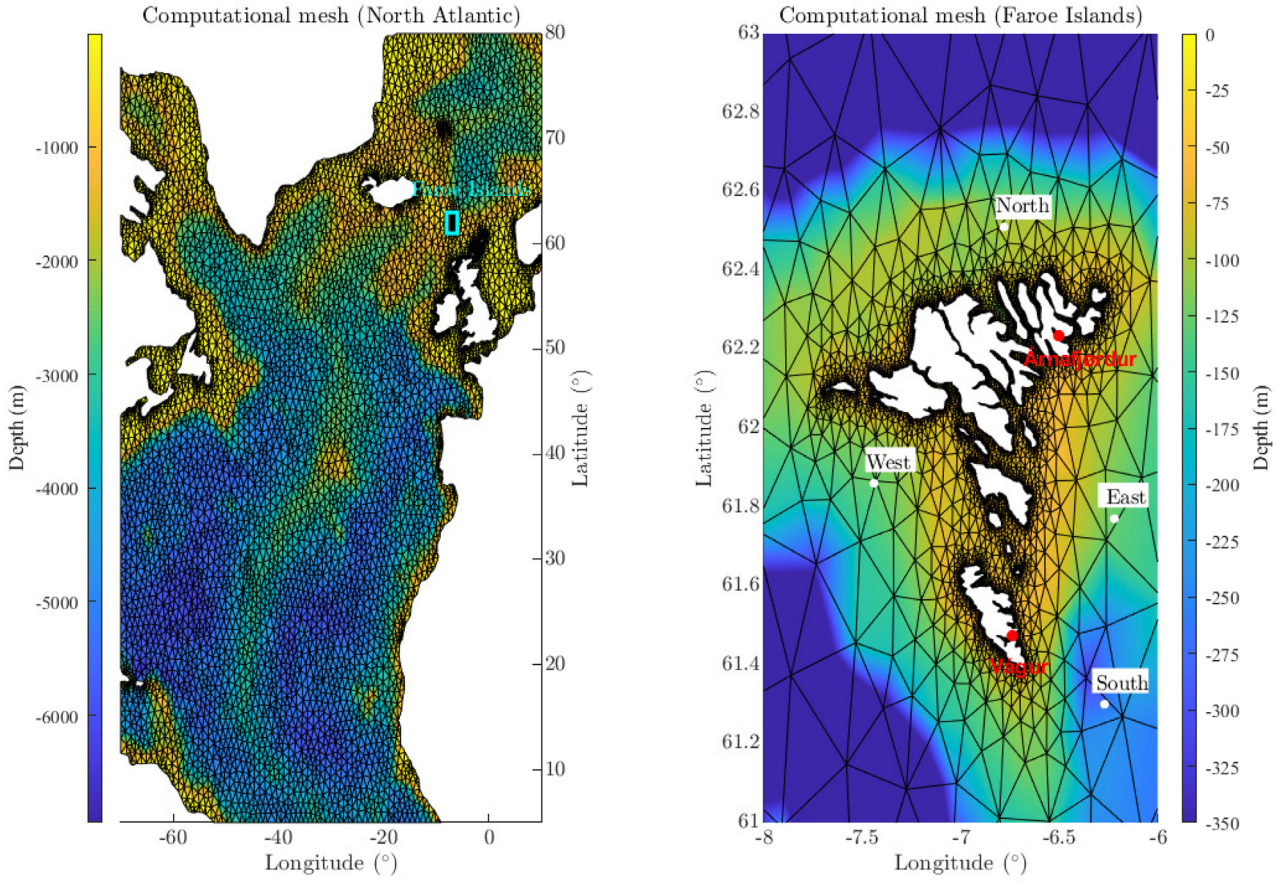

(a) North Atlantic computational mesh and bathymetry.

(b) Mesh and bathymetry around the Faroe Islands.

Fig. 1. The computational domain and mesh for the study area. (a) The North Atlantic, (b) the Faroe Islands together with wave measurement points.

Due to computational constraints, high resolution was only applied for the area around the Faroe Islands, where local bathymetry data was used [49], consisting of 100 m by 100 m data points. It was desirable to have a higher resolution of data, however this was not available. A filter was applied for the whole area (excluding 8°W to 6°W and 61°N to 63°N), such that the resolution of the bathymetric data for the rest of the North Atlantic was 1° latitude by 1° longitude.

The model domain consists of 19983 elements at various mesh resolutions, with the area around the Faroe Islands having the finest resolution and the North Atlantic ocean with the coarsest resolution. The mesh element area varies from $1.9 \cdot 10^4 km^2$ to $3.7 \cdot 10^{-3} km^2$ and the grid for the output results is the same resolution as the input mesh in Fig. 1 (b).

3.2. Model forcing and model settings

The model was forced with data for the wind speed at 10 m above sea level and its direction, acquired from the re-analysis dataset (ERA5) from the European Center for Medium range Weather Forecast (ECMWF) climate data store (CDS) [29]. This has a spatial resolution of 0.25°x0.25° and a temporal resolution of 1 hour. The ERA5 model reanalysis results will be used as an accepted state of the art reference for our region, since it is a model known to give acceptable local forecasts [50].

For the frequency discretization, a logarithmic discretization is used with a minimum frequency of 0.035 Hz, with 40 frequencies and a frequency factor of 1.1, see Ref. [28] for further details. For the directional discretization, 24 directions are used with each direction covering 15°.

As a default setting for the instationary formulation solution technique a 'lower order' geographical space discretization algorithm is used, with 'maximum number of levels in transport' of 32, where 'lower order' means a first order upwinding numerical

Table 1
Model forcing and physical processes activated in model.

Physical process/Set up	Value
Spectral formulation	Fully spectral
Time formulation	Instationary
Number of directions	24
Number of frequencies	40
Water level variation	No
Current conditions included	No
Ice coverage	No
Diffraction	No
Quadruplet wave interaction	Yes
Triad wave interaction	Yes
Wind forcing	ERA5 0.25x0.25° 10 m speed & direction
Depth-induced wave breaking	$H/h = 0.8$
Bottom friction	Nikuradse roughness, $k_N = 0.04$
White-capping	$C_{dis} = 1.9$ & $\delta_{dis} = 0.6$
Initial conditions	Zero spectra

scheme. No water level variation, current conditions, ice coverage or diffraction were included in the model. A point, located a few hundred meters south of the southernmost island was used for comparison for initial test runs to see the effect of including the diffraction. There was basically no difference in the significant wave height, peak wave period, wave direction or the wave power.

As a starting point, default settings were applied to the model. However, for the white-capping source term, the recommendation from Ref. [51] was applied, since we are dealing with a combination of wind-sea and swell. Initial model runs with the recommended value showed that the model underestimated the significant wave height, showing that the dissipation of energy due to white-capping was initially too high. Therefore, the dissipation coefficient C_{dis} was changed from the recommended value of 2.1 to 1.9. Table 1 shows the model forcing and physical processes activated in the model.

3.3. Wave data measurements used for validation of the model

All of the near-shore data used, has been provided by Fiskaaling (www.fiskaaling.fo). This data is collected with Acoustic Doppler Current Profilers (ADCP). These are mainly used for current measurements, but they can be used, for wave measurements as well. They are deployed in shallow water, since the measuring device has to be submerged at a limited depth in order to measure with sufficient accuracy [52].Four offshore 0.9 m diameter directional Datawell Waverider buoys are also used in the validation, see Fig. 1 (b). The first wave buoys were deployed in 1980 [53,54], and these have been a part of the local operational services for fishermen.

3.4. Validation of the MIKE 21 SW model

A comparison between the calculations from MIKE 21 SW and the measurements made at different locations around the islands is crucial in order to quantify the validity of the wave model. The Árnafjørdur and Vágur measurement locations are nearshore locations, while the east, north, west and south locations are offshore locations. The first two are associated with aquaculture in the Faroe Islands, and the others are owned and operated by Landsverk [55]. Fig. 1 (b) shows a map of the locations of the performed measurements. The model validations are performed over different time periods, because the nearshore location data only spans a few months recorded over a few different periods, while the measurements from Landsverk are large datasets which cover several decades. To quantify the validity of the wave model, statistical parameters such as bias, root-mean-square error (RMSE), scatter index (SI) and correlation coefficient (R) are calculated.

$$\text{Bias} = \frac{1}{N}\sum_{i=1}^{N}(x_{m_i} - x_{o_i}) \tag{3}$$

$$\text{RMSE} = \sqrt{\frac{1}{N}\sum_{i=1}^{N}(x_{m_i} - x_{o_i})^2} \tag{4}$$

$$\text{SI} = \frac{\text{RMSE}}{\bar{x}_o} \tag{5}$$

$$\text{R} = \frac{\sum_{i=1}^{N}(x_{m_i} - \bar{x}_m)(x_{o_i} - \bar{x}_o)}{\sqrt{\sum_{i=1}^{N}(x_{m_i} - \bar{x}_m)^2 (x_{o_i} - \bar{x}_o)^2}} \tag{6}$$

where x_o is the observed (measured) data and x_m is the model data with mean values $\bar{x}_o$ and $\bar{x}_m$ respectively. Bias gives information on whether the model over- or underestimates the modeled parameter, RMSE gives information on the differences between the observed and modeled values (residuals). The scatter index SI puts the RMSE in a relative frame (non-dimensional), the correlation coefficient R measures the linear correlation between the modeled and measured values. The validation parameters for the wave direction are not calculated using a linear approach, which might yield misleading results, especially when considering waves traveling from a northern direction (0° and 360°). Instead, a vectorial approach is applied, taking the distance between each wave direction component (modeled and measured) to calculate the validation parameters.

Table 2
Validation parameters for measurements and MIKE model comparison.

Site	Parameters	Bias	RMSE	SI	R
East	H_{m0} [m]	−0.06	0.37	0.17	0.95
	T_p [s]	−0.56	1.78	0.20	0.75
	Dir_p [°]	24.71	32.29	0.26	0.68
West	H_{m0} [m]	−0.19	0.52	0.19	0.98
	T_p [s]	−0.23	2.05	0.20	0.70
	Dir_p [°]	22.17	30.33	0.12	0.64
North	H_{m0} [m]	−0.19	0.47	0.19	0.96
	T_p [s]	−0.22	1.48	0.15	0.82
	Dir_p [°]	21.05	28.63	0.14	0.62
South	H_{m0} [m]	−0.11	0.42	0.17	0.97
	T_p [s]	−0.26	1.37	0.14	0.85
	Dir_p [°]	20.30	28.23	0.15	0.60
Árnafj.	H_{m0} [m]	0.05	0.23	0.26	0.96
	T_p [s]	0.10	2.00	0.24	0.53
	Dir_p [°]	22.95	32.26	0.26	−0.18
Vágur	H_{m0} [m]	−0.03	0.15	0.24	0.96
	T_p [s]	0.61	2.49	0.32	0.47
	Dir_p [°]	23.78	30.01	0.32	0.35

Table 2 shows the validation parameters for the considered locations (see Fig. 1(b)). H_{m0} is the significant wave height, T_p is the peak wave period and Dir_p is the peak wave direction. For the east and south locations there is agreement between the modeled and measured significant wave height, however the model slightly under predicts the significant wave height. For the peak wave period, there is some discrepancy between the modeled and measured data. There is a reasonably low scatter value and a fairly high correlation. For the west and north location, there is some deviation between the modeled and measured data, for both the significant wave height and the peak wave period. However, the scatter index is quite low and there is generally a good correlation between modeled and measured data.

For the Árnafjørdur and Vágur locations, agreement is found between the modeled and measured data, however for the peak wave period some deviations are found. Wave direction shows larger discrepancies between modeled and measured, compared to offshore locations.

Fig. 2(a) and Fig. 2(b) show scatter plots for significant wave height and peak wave period for the east and west locations, for the time period 01-01-2012 to 31-12-2012. The figures show that the model is capable of capturing the measured significant wave height data quite well. The majority of the peaks in significant wave height are captured by the model, however for some of the sharp peaks the model underpredicts the significant wave height. For the peak wave period there is more scatter, but the majority of the data is well-captured by the model.

Fig. 2(c) and (d) show scatter plots of the modeled and measured significant wave height and peak wave period at the north and south locations, for the period 01-04-13 to 31-12-13. The model captures the significant wave height well at both

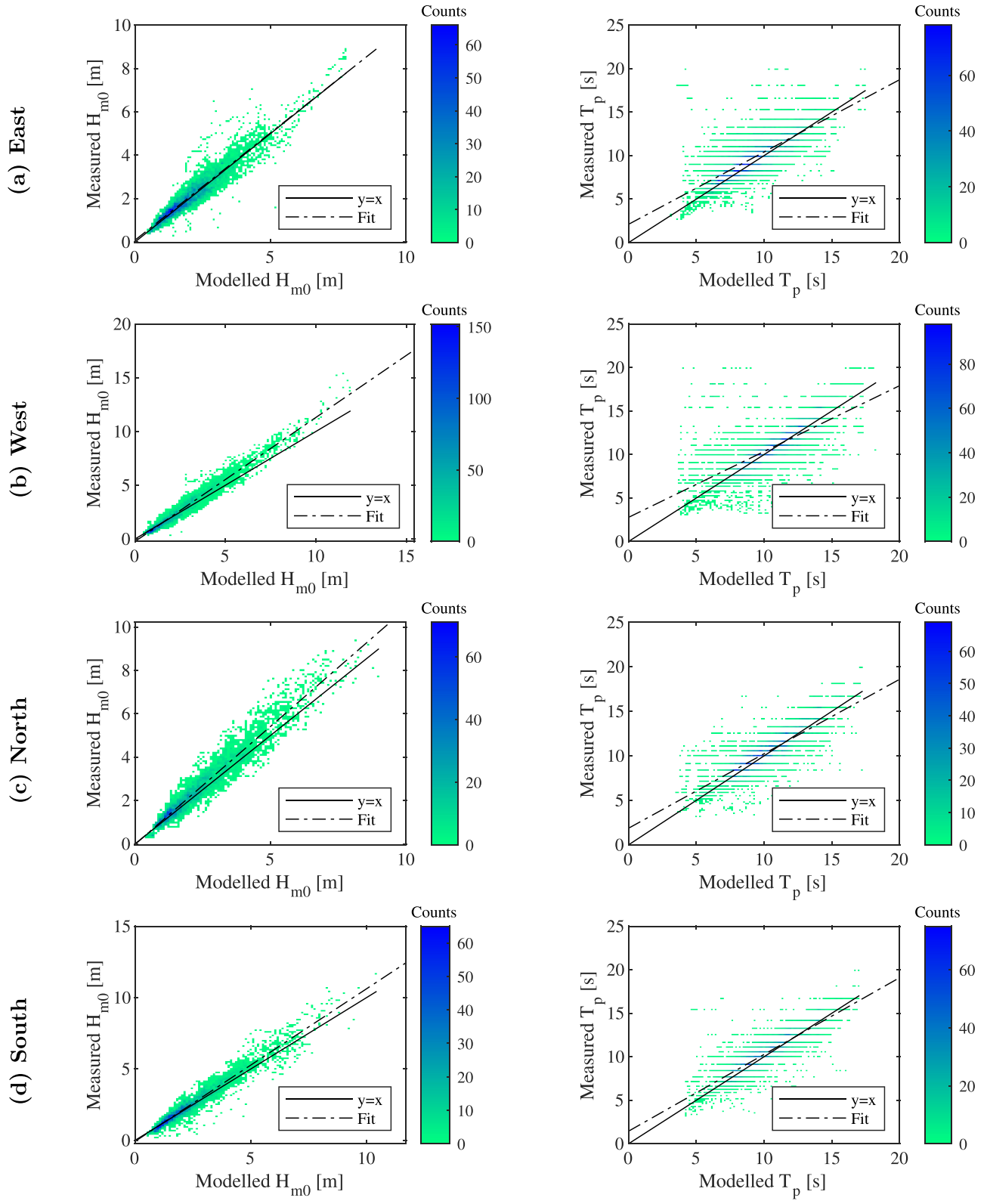

Fig. 2. Scatter plots. (a) Significant wave height H_{m0} (left) and peak wave period (right) for the east location, (b) Significant wave height H_{m0} (left) and peak wave period (right) for the west location, (c) Significant wave height H_{m0} (left) and peak wave period (right) for the north location, (d) Significant wave height H_{m0} (left) and peak wave period (right) for the south location.

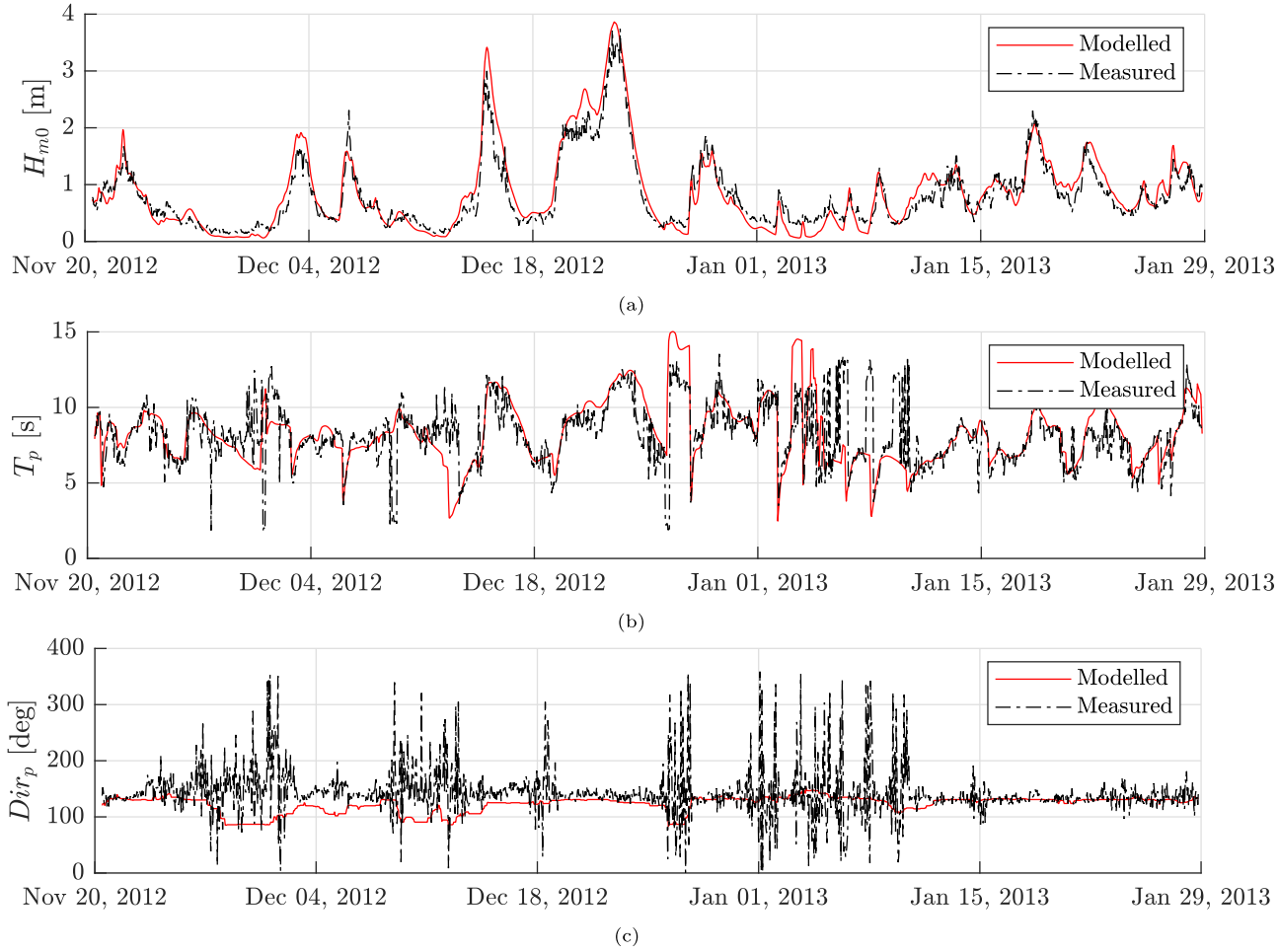

Fig. 3. Time-series of modeled and measured (a) significant wave height, (b) peak wave period and (c) peak wave direction for the Árnafjørdur location, model validation phase.

measurement locations. However, some of the peaks in the wave height are underpredicted by the model. For the peak wave period there is a bit more scatter in the comparison data, but the majority is captured by the model.

The validation statistics at the offshore buoys show comparable levels of accuracy at the different sites around the islands. However, there are discrepancies in the peak wave direction, especially for bias and RMSE. The east site has the highest level of sheltering, so an undershoot in the modeled peak wave period could indicate that the modeled sheltering was too strict compared to reality.

Fig. 3 and Fig. 4 show the time-series of the significant wave height, peak wave period and the peak wave direction for the Árnafjørdur and Vágur locations used for validating the model. The figures show agreement between model and measurements, and the majority of the peaks in significant wave height are captured by the model. There are discrepancies for the peak wave period at both locations. For the wave direction at the Árnafjørdur location, the model captures this for the majority of the time. However, in the measurements, there is a lot of spreading in the wave direction for the smaller significant wave heights. This could be caused by the fact that when a state of small waves is present, the measurement device captures waves coming from many more directions, than what is captured in the model, or that the device needs a certain signal to noise ratio, i.e. wave height, before making valid wave direction measurements. Figs. 3 and 4 show that the larger wave heights contain a more consistent wave direction, compared to the smaller wave heights. Fig. 4 shows the same phenomenon as described above for the Vágur location. However, there are larger deviations at the Vágur location than at the Árnafjørdur location. The mean wave directions in the Árnafjørdur and Vágur locations are 138° and 112°, respectively. Keeping in mind that the Árnafjørdur fjord's opening, faces in a southeastern direction and the Vágur fjords opening faces an east-southeast direction, it makes sense that the majority of the waves travel from these above mentioned directions.

One thing all of the above mentioned validation studies have in common, is the comparison quality of the peak wave direction. In all of the cases, there is quite a large deviation between the measured and the modeled data. The peak wave direction is a sensitive parameter, as it describes where the most energetic wave comes from. Furthermore, there is usually a lot of scatter associated with the peak wave direction. Unfortunately, the mean wave direction was not available from the measurements (only peak wave direction was available), as this would have introduced a more consistent wave direction, and probably given less scatter.

Mesh resolution might also play a role in the accuracy of the modeled direction compared to the measured, considering that sheltering zones might need an even higher resolution than what was applied here.

As mentioned earlier, it is of great importance to ensure the quality of the model results. Parameters such as bias and RMSE are often used for quality checks. Ref. [27] found bias values for H_{m0} ranging from −0.16 m to 0.27 m and RMSE as high as 0.45 m. Ref. [30] found bias values for H_{m0} around −0.06 m and RMSE as high as

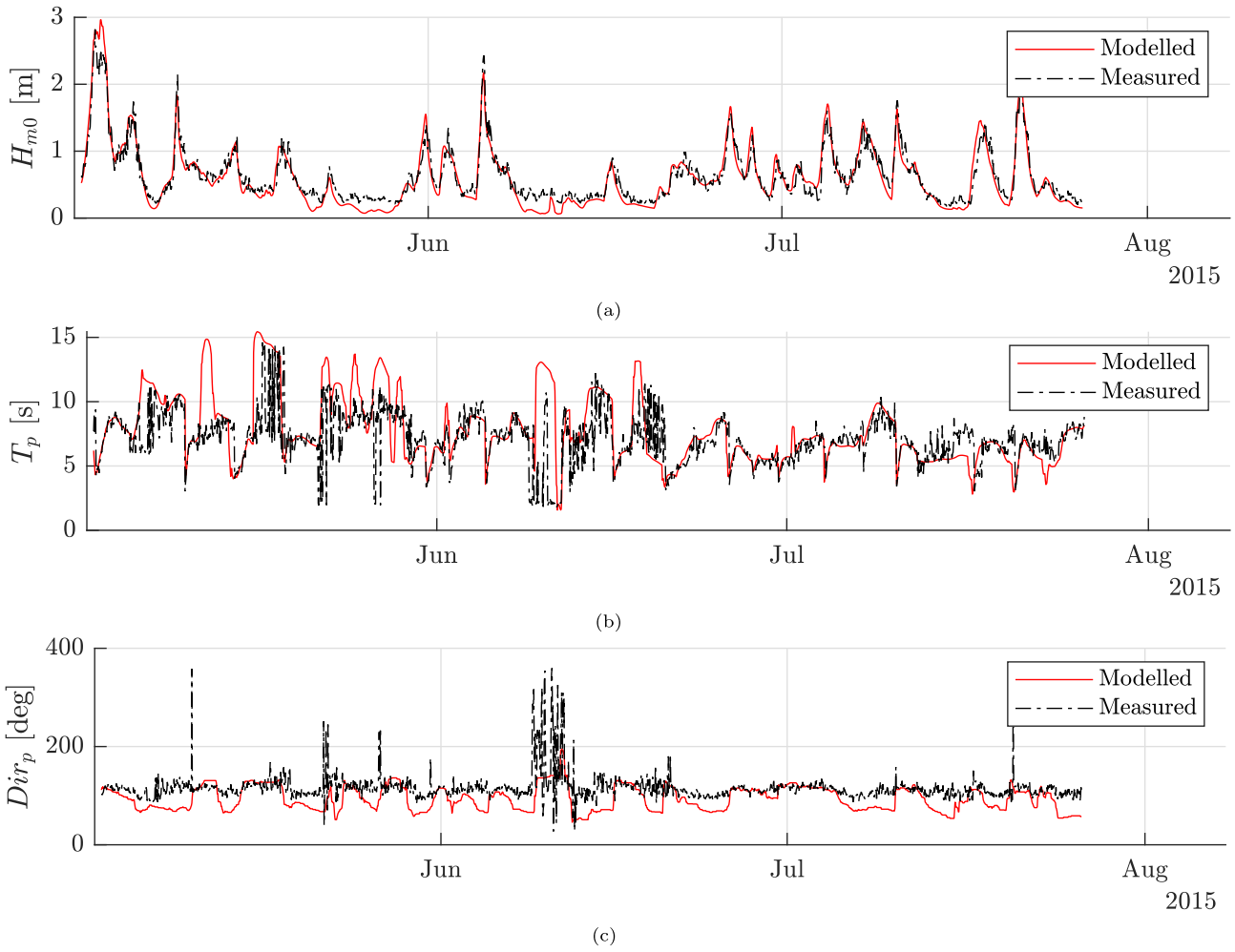

Fig. 4. Time-series of modeled and measured (a) significant wave height, (b) peak wave period and (c) peak wave direction for the Vágur location, model validation phase.

0.71 m. Ref. [31] found bias values for H_{m0} ranging from −0.01 m to −0.13 m and RMSE as high as 0.60 m. The present study shows bias values from 0.06 m to 0.19 m for the offshore locations and −0.05 m to 0.03 m for the nearshore locations. RMSE values ranging from 0.37 m to 0.52 m for the offshore locations and RMSE values of 0.15 m and 0.23 m for the nearshore locations, respectively. This leads us to conclude that the model quality is comparable to similar recent studies in the literature.

4. Results and discussion

4.1. Wave hindcasting

As the model is thoroughly validated and is able to predict the wave parameters efficiently, the next step is to investigate the spatial variation of the wave climate around the Faroe Islands. This is represented in terms of the significant wave height and the average wave energy flux. These parameters will be presented as annual mean and maximum, together with seasonal mean variation.

Fig. 5 shows the mean significant wave height for the ten year period 01-01-2009 to 31-12-2018 for the Faroese waters. The figure shows that the western and northern coasts contain higher waves than the eastern coasts. Values of about 2.4 m−3.0 m significant wave height on the western and northern coasts, and values of about 1.2 m−2.0 m in the eastern coasts.

Fig. 6 shows the maximum significant wave height for the period 01-01-2009 to 31-12-2018. A similar trend is seen here as in Fig. 5, higher waves on the western and northern coasts compared to the eastern coast. Values of about 12−14 m at the western coasts, 9−13 m at the northern coasts and about 8−9 m at the eastern coasts. We note that these results compare well with what was found in Ref. [41].

The wave energy flux, or wave power, in a sea state in arbitrary water depth, can be expressed as

$$P = \rho g \int_0^{2\pi} \int_0^{\infty} E(\sigma,\theta) c(\sigma,\theta) \mathrm{d}\sigma \mathrm{d}\theta \tag{7}$$

where $E(\sigma, \theta)$ is the energy density, $c(\sigma, \theta)$ is the group velocity, ρ is the density of water and g is the gravitational acceleration. Fig. 7 shows the mean wave energy flux calculated from Equation (7). This figure shows the same trends as the previous figures. The wave energy flux at the western and northern coasts contain a higher amount of energy than the eastern coasts. Values of wave energy flux at the western and northern coast vary from 45 kW/m to 55 kW/m. At the eastern coast the values vary from 10 kW/m to 25 kW/m.These results for the wave energy flux correspond well with what is presented in Ref. [40] in terms of the spatial variation of wave energy flux. The results in Ref. [40] are derived from the four wave measurement buoys west, south, east and north shown

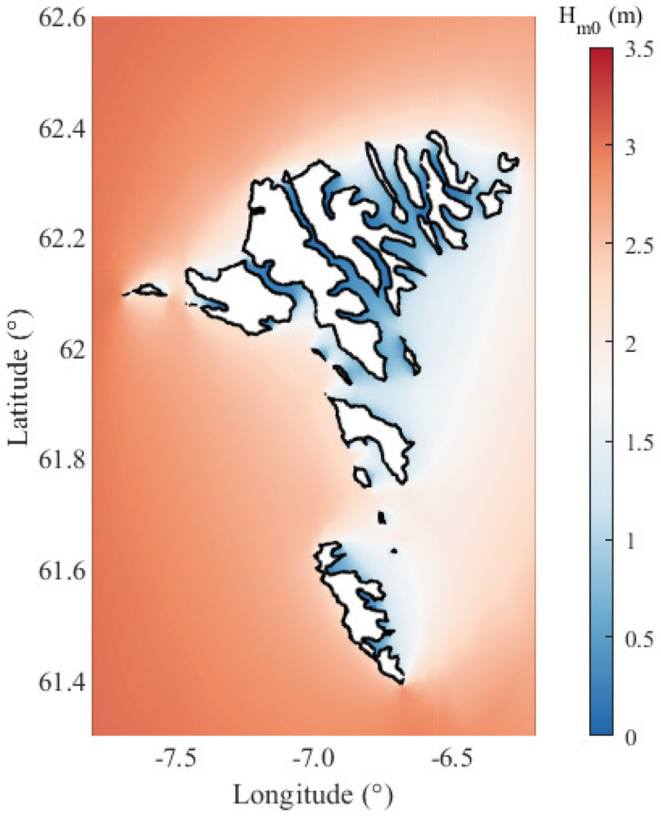

Fig. 5. Mean significant wave height for January 2009 to December 2018.

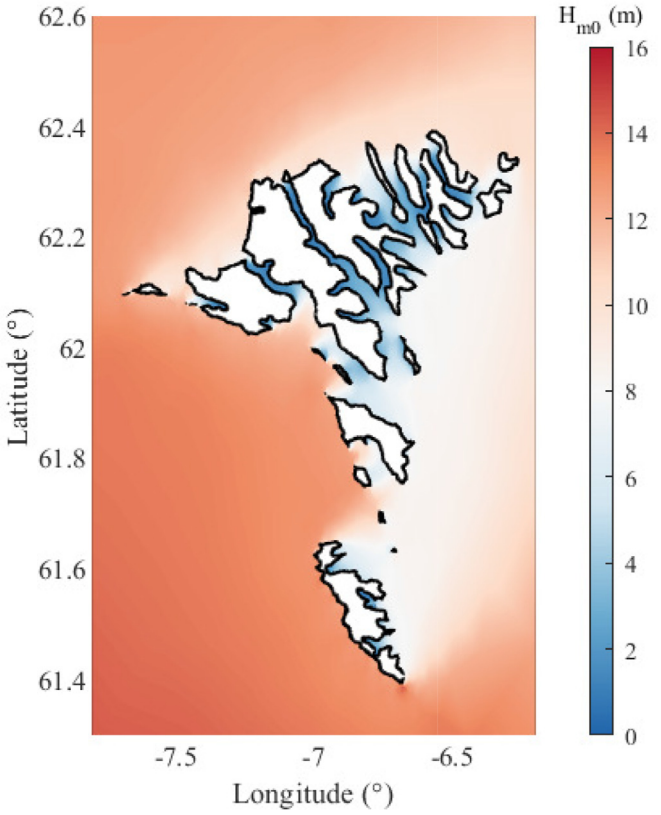

Fig. 6. Maximum significant wave height for January 2009 to December 2018.

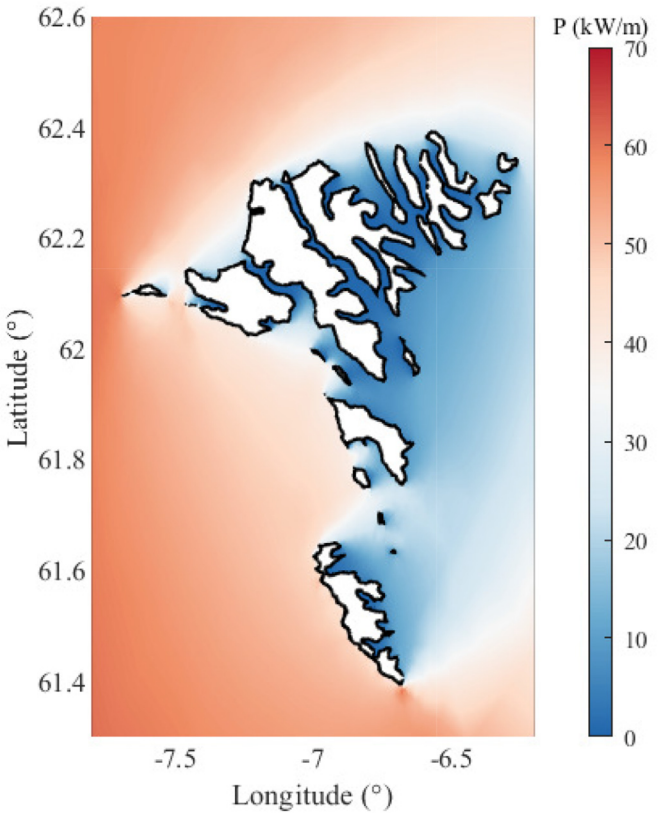

Fig. 7. Mean wave energy flux for January 2009 to December 2018.

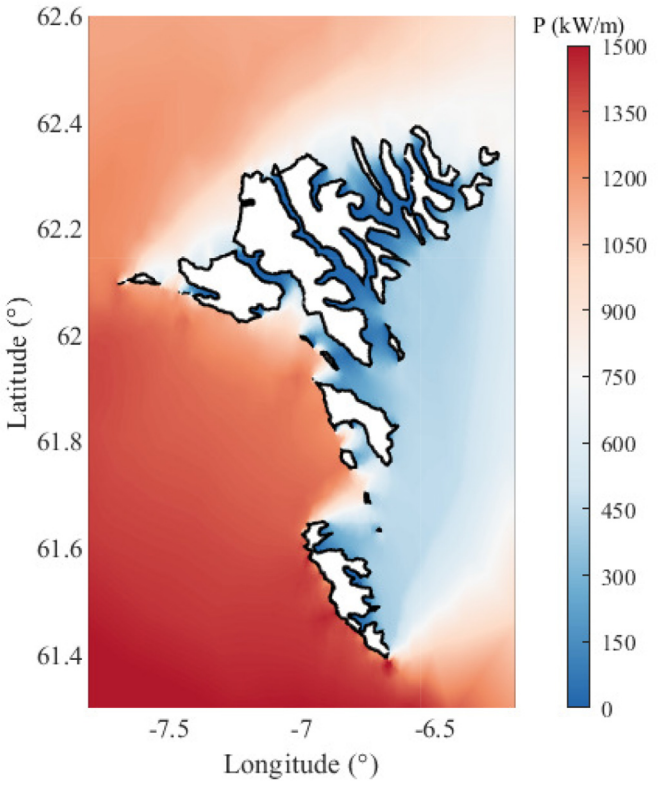

Fig. 8. Maximum wave energy flux for January 2009 to December 2018.

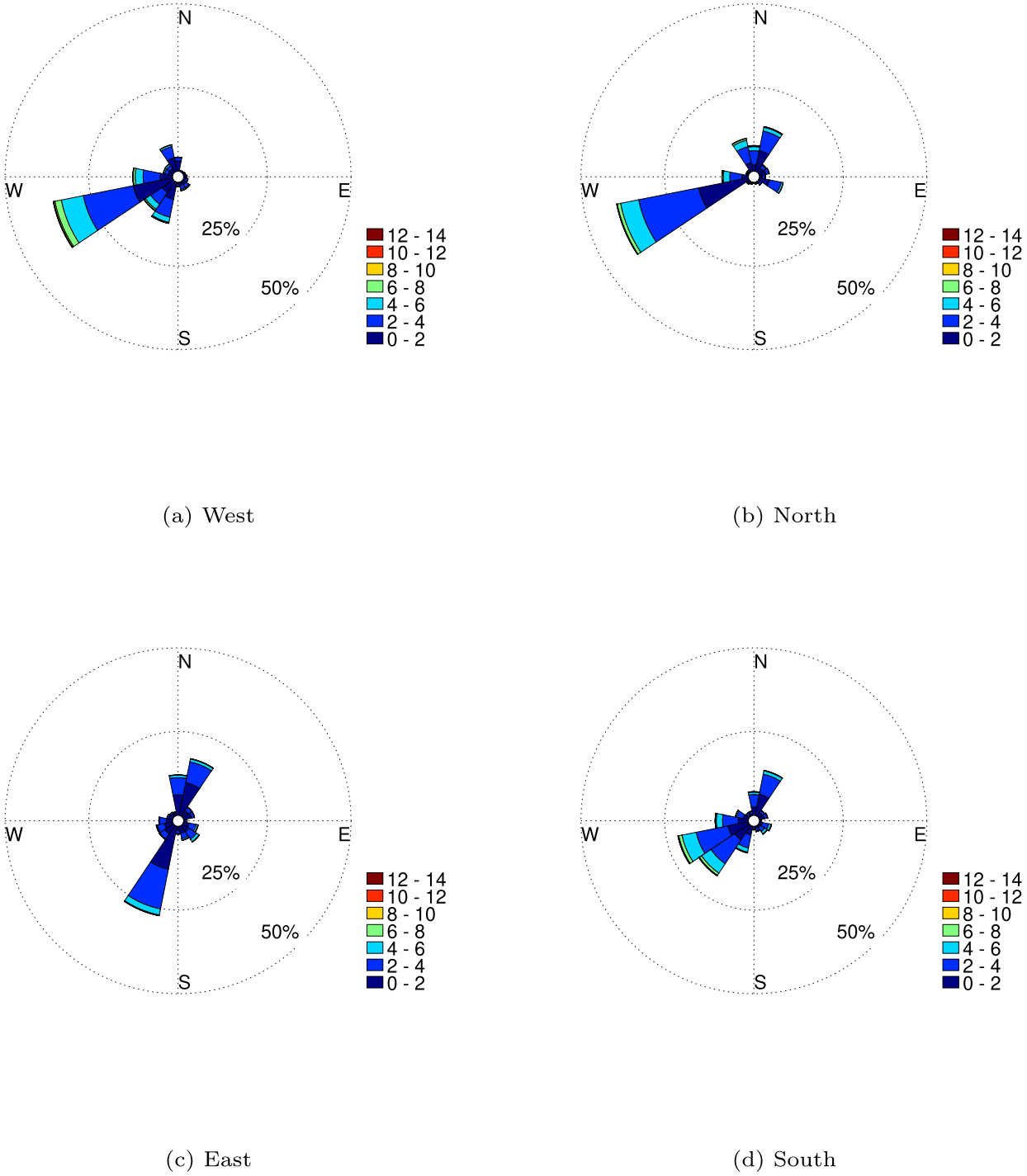

Fig. 9. Wave rose plots for the four offshore buoy locations - model results. (a) West, (b) North, (c) East and (d) South.

in Fig. 1(b).

Venugopal et al. [27] presented maps of average wave energy flux for Scottish waters. Keeping in mind that the Faroe Islands are located directly north of Scotland, the statistical values in that study are aligned with what is found in the present study. However, the values for average wave energy flux in the present study are higher closer to shore.

Fig. 8 shows the maximum wave energy flux around the Faroe Islands. Values of 1200–1500 kW/m along the western coast, 600–1000 kW/m on the northern coast and on the eastern coast, values of 300–600 kW/m.

4.2. Wave direction

As this is a study of wave power potential and it investigates the possibilities of deploying wave energy devices in the Faroe Islands, it is important to look at which direction the waves come from. To this end, wave rose plots have been compiled in order to visualize

where the majority of the waves travel from.

Fig. 9 shows wave rose plots for the four offshore locations - west, east, south and north. For the west and south location, the majority of the waves travel from a west and southwesterly direction. This makes sense, since the majority of the storms that hit the Faroes travel from the mid North Atlantic Ocean. For the north location the majority of the waves travel from the west and north. The north buoy measurement location is not in a sheltered zone, when storms travel from the mid North Atlantic (southwest direction), hence the large number of occurrences from the west. The north location also shows high occurrence from the north, while the west and south locations do not to the same extent. This is natural, since these buoys are largely sheltered from waves coming from the north.

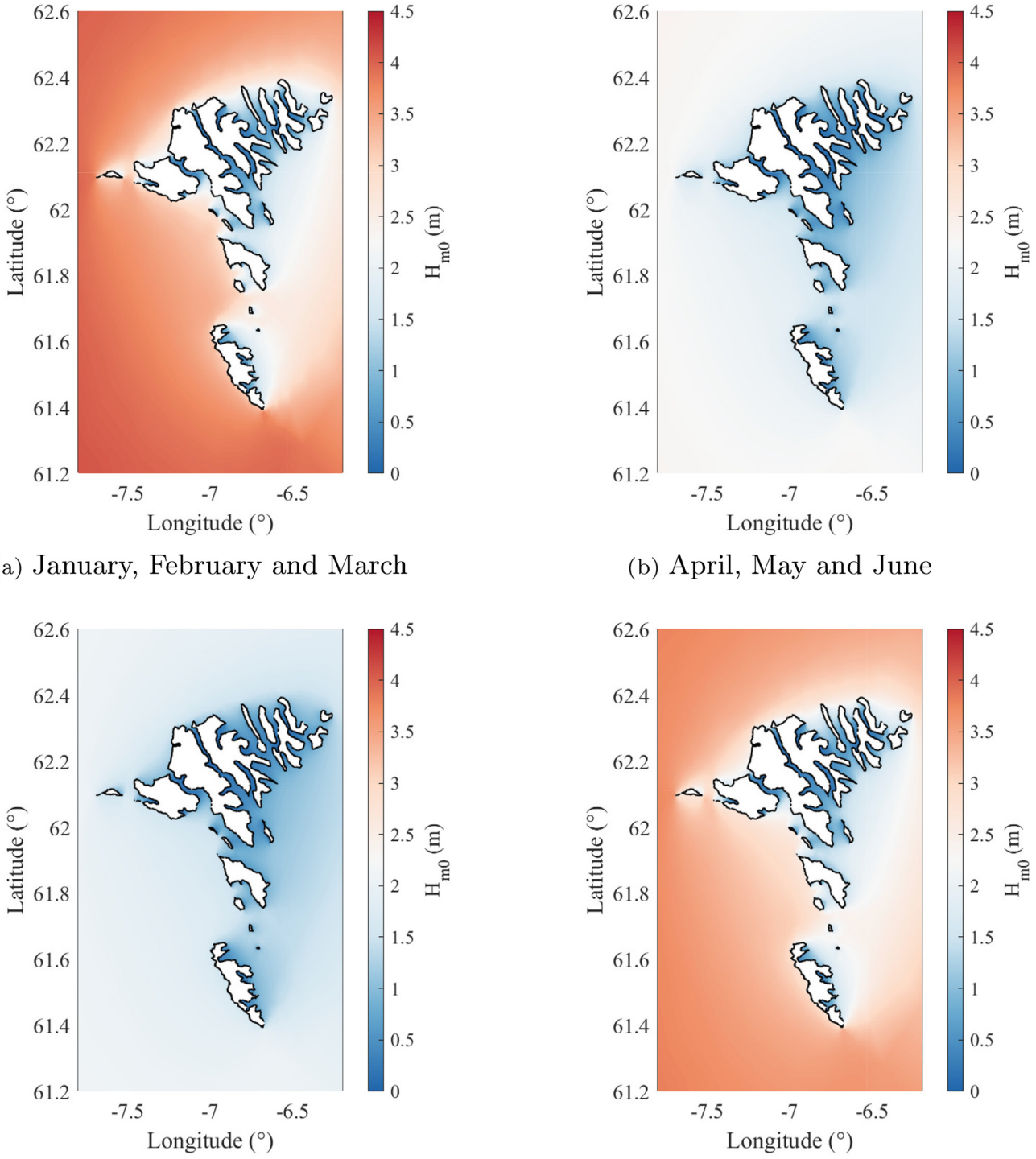

(a) January, February and March

(b) April, May and June

(c) July, August and September

(d) October, November and December

Fig. 10. The seasonal variation of the mean significant wave height of the four considered seasons. (a) January, February and March, (b) April, May and June, (c) July, August and September, (d) October, November and December.

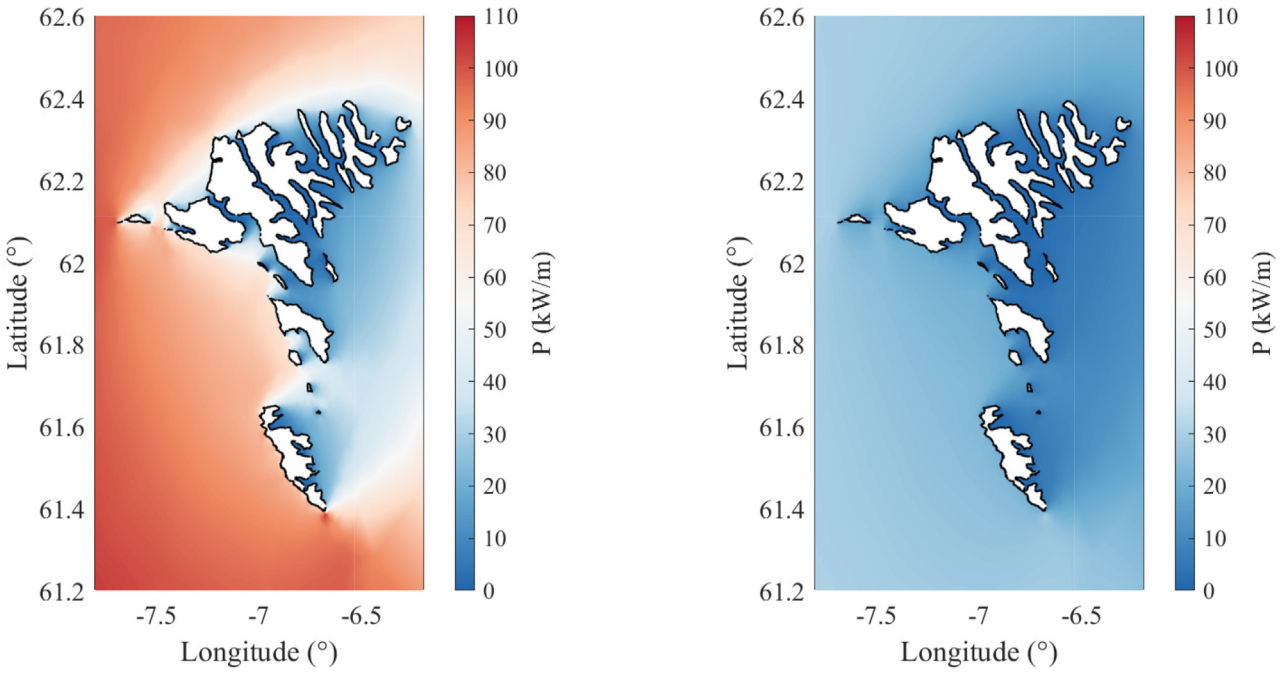

(a) January, February and March

(b) April, May and June

(c) July, August and September

(d) October, November and December

Fig. 11. The seasonal variation of the mean wave energy flux of the four considered seasons. (a) January, February and March, (b) April, May and June, (c) July, August and September, (d) October, November and December.

For the east location the majority of the waves come from the north and south directions. If waves travel to the Faroes from a southwestern direction these will be refracted around the southern most island and be seen on the east location as traveling from a nearly southerly direction.

4.3. Seasonal variation

As the Faroe Islands are located in the North Atlantic Ocean, there are relatively large seasonal variations in the wave climate. Harsh and rough seas are normal in autumn and winter, while towards the end of spring and in summer, the seas are usually much calmer. Therefore, it is of great interest to analyze how large these

variations in the wave climate are from season to season. In this study we look at each season as a three month period, starting with January. Fig. 10 shows the variation in the mean significant wave height, in each season.The figure shows, that the mean significant wave height in the winter and autumn period is much higher than in the spring and summer months. For the winter and autumn months, the mean significant wave height is 3–4 m at the western and northern coasts and 1.5–2.5 m at the eastern coasts. In the spring and summer months, the mean significant wave height is 1.5–2 m at the western and northern coasts and 0.8–1.4 m at the eastern coasts.

The seasonal variation of the average wave energy flux around the islands is shown in Fig. 11. It is clear that the wave energy flux is higher in the autumn and winter months, compared to the spring and summer months.The values are 70–80 kW/m on the western and northern coasts during the autumn and winter months, and 25–35 kW/m on the eastern coasts. The wave energy flux in the spring and summer months varies between 20 kW/m and 30 kW/m along the western and northern coasts, and at the eastern coasts the wave energy flux is 5–10 kW/m.

4.4. Evaluation of the local energy potential

Information on the energy content, peak periods and wave direction is vital, at the first stage of consideration of potential wave energy device deployment. As a first step, we have selected a series of target deployment locations where we evaluate the local energy potential. Here only 3 points are investigated in more detail, as these are representative for the given offshore areas. One point is selected in the western waters, one point in the eastern waters and one point in the northern waters. In practical terms, it is important to know how much each sea-state contributes to the total available wave energy. Figs. 12–14 show the yearly average energy at each of the selected locations, along with the energy period (T_e) and the significant wave height (H_{m0}). The intensity of the colorbar shows the annual energy contribution in (MWh/m) and the numbers on the figure show the yearly average occurrence frequency of each sea-state. Isolines for the average wave energy flux are also shown.

The occurrence frequency of each sea-state is calculated by ordering the energy period (T_e) and the significant wave height (H_{m0}) in bins and counting how frequently these occur on average per year for the time period 2009–2018. The average wave energy flux is calculating using a parametrized version of Equation (7), depending on the energy period (T_e), the significant wave height (H_{m0}), the wave number based on the energy period (k_e) and the water depth h.

$$P = \frac{\rho g^2}{64\pi} H_{m0}^2 T_e \left(1 + \frac{2k_e h}{\sinh(2k_e h)}\right) \tanh(k_e h) \tag{8}$$

For the annual mean wave energy in (MWh/m) the average wave energy flux is multiplied by the hourly occurrence p_{hourly} of each sea state (H_{m0}, T_e).

$$P_{annual} = P \cdot p_{hourly} \tag{9}$$

Figs. 12–14 show that there is a higher energy content in the western and northern coasts, compared to the eastern coast. The occurrence of sea-states with shorter and smaller waves are more frequent in the eastern lying point, compared to sea-states with longer wave periods and larger wave heights dominating at the western and northern points. As a starting point, it is of course beneficial to consider sites with high energy content as these will yield a high energy production. However, considering the scatter diagram in Fig. 12, we see that the high energy content is contained in sea-states with long wave periods and large wave heights. This will in the end lead to larger wave forces, leading to stricter design considerations. Preferably, we would want the high energy content located in the "milder" sea-states, leading to a more stable production of energy.

Considering the different types of concepts for wave energy

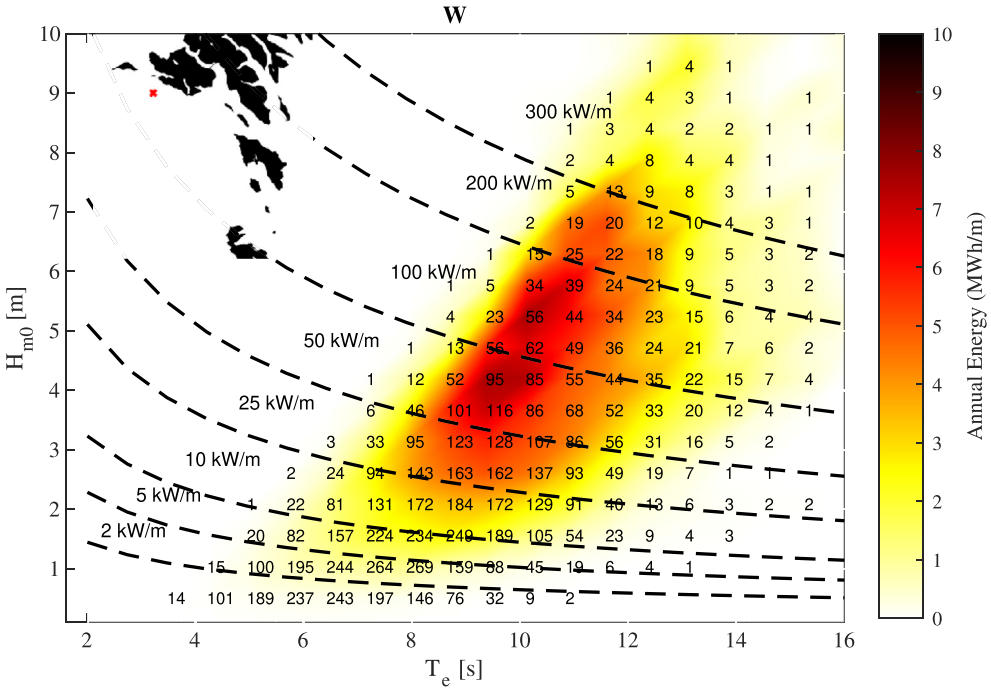

Fig. 12. Annual mean wave energy in (MWh/m) at point W, presented in terms of significant wave height H_{m0} and energy period T_e. The numbers on the plot show the occurrence per year of each sea state.

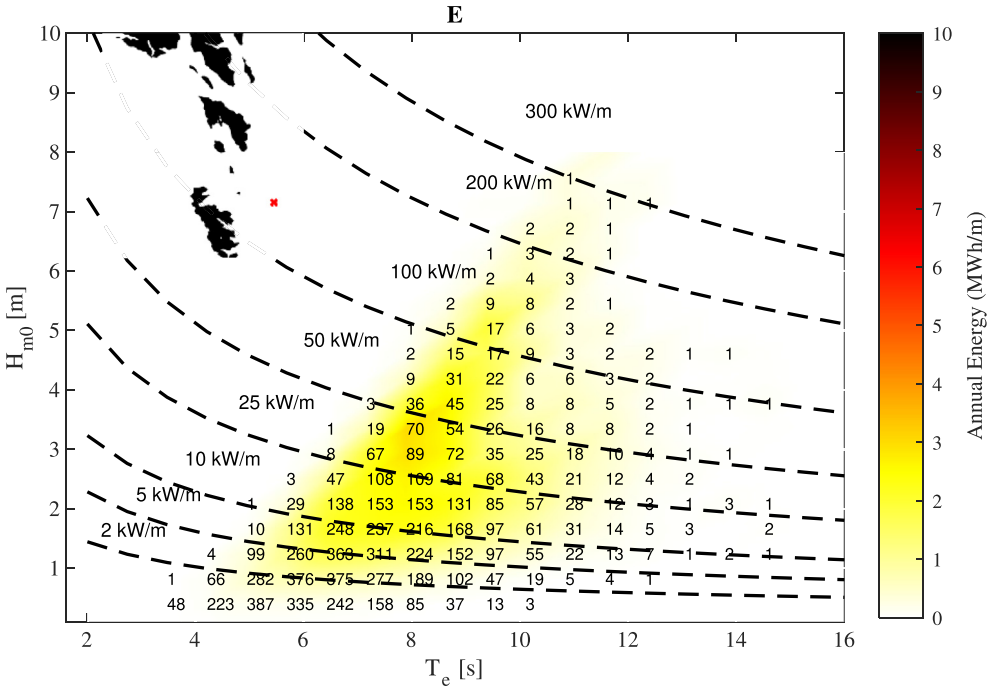

Fig. 13. Annual mean wave energy in (MWh/m) at point E, presented in terms of significant wave height H_{m0} and energy period T_e. The numbers on the plot show the occurrence per year of each sea state.

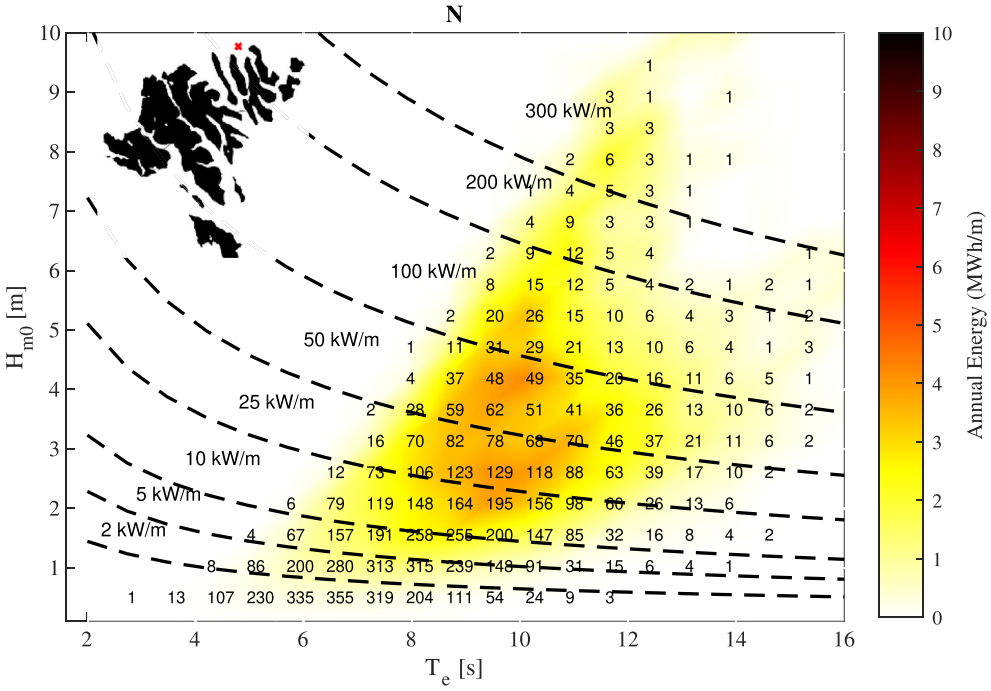

Fig. 14. Annual mean wave energy in (MWh/m) at point N, presented in terms of significant wave height H_{m0} and energy period T_e. The numbers on the plot show the occurrence per year of each sea state.

extraction, we would like to choose a design for the specific site so that the resonance wave period has a high representation in the scatter diagram. The more frequently the resonance period is represented the higher the energy output is from the device.

Table 3 shows the annual average energy content in MWh/m, the water depth and the distance to shore for each of the considered sites. The table shows the same trend as in Figs. 12–14, that the energy content is much higher at the western location, compared to eastern and northern. All three points have a relatively large water depth, when considering wave energy extraction devices, therefore floating devices are the most probable type to be installed at each location. The distance to shore varies a lot from site

Table 3
Annual average energy content, water depth and distance to shore for each of the considered sites.

Site	Annual energy	Depth	Distance to shore
[−]	[MWh/m]	[m]	[m]
W	424.9	77	5490
E	160.3	66	8650
N	264.5	89	3400

to site, giving a variation in installation costs, considering power transmission to land. However, at the northern location, the distance to shore is relatively short compared to the other locations, but the nearest islands all contain large headlands on the northern facing sites. So the actual power cable length from the north location to the nearest realistic land location is probably twice the distance shown in Table 3.

Indeed there are many things to consider before deployment of any type of wave energy extraction device. From a strict annual average energy content point of view, the western location is indeed the preferable one. However, at this location the occurrence of extreme sea-states is higher than at the other sites, leading to a longer survival mode operating time, and possibly also leading to more wear and tear on the device. If a more moderate production is desirable, the east location will be preferable, since the occurrence of milder sea-states is higher at this location.

5. Conclusions

This work developed a large scale model of the North Atlantic ocean, using the state-of-the-art wave model suite MIKE 21 SW, for hindcasting of wave parameters, specifically for the waters around the Faroe Islands. The model was forced by wind data from ECMWF at 0.25°x0.25° resolution. Furthermore, a comprehensive validation was performed using measured wave data from wave buoys both offshore and nearshore around the Faroe Islands. The validation study for the offshore buoys showed that the significant wave height was successfully reproduced, with correlation coefficients higher than 0.95. For the nearshore locations, correlation coefficients for the significant wave height were 0.96. For the peak wave period at the offshore locations, this was somewhat successfully reproduced, with correlation coefficients varying from 0.7 to 0.85. However, for the nearshore locations, the peak wave period showed higher discrepancies, with correlation coefficients of 0.53 at the Árnafjørdur site, and 0.47 at the Vágur site.Results for the statistical maximum of the significant wave height, were in agreement with a previous study [41]. Values of 12–14 m were found at the western coasts, 9–13 m at the northern coasts and 8–9 m at the eastern coasts. Furthermore, results for the annual average wave energy flux aligned with what was presented in Ref. [40], showing 45–55 kW/m at the western and northern coasts, and 10–25 kW/m at the eastern coasts.

The results of the present study show that the developed wave model can be used with high confidence to provide detailed wave statistics at suitable locations in the Faroe Islands. This will provide valuable data for initial design studies on the deployment of wave energy converters for power production and the transition to a 100% renewable supply.

Credit author contribution statement

Bárður Joensen: Conceptualization, Methodology, Validation, Formal analysis, Investigation, Data curation, Writing – original draft, Writing – review & editing, Funding acquisition, Bárður A. Niclasen: Writing – original draft, Writing – review & editing, Supervision, Harry B. Bingham: Writing – original draft, Writing – review & editing, Supervision, Project administration.

Declaration of competing interest

The authors declare that they have no known competing financial interests or personal relationships that could have appeared to influence the work reported in this paper.

Acknowledgements

This study is based on project supported by the Research Council of the Faroe Islands, grant number 02010. The same project is also financially supported by Betri Bank and SEV. The authors would like to thank Landsverk and Fiskaaling for providing the measured wave data.

References

[1] Vinnuhúsið-anonymous. Tech. rep.. In: Notat um elprísirnar til føroyskar ídnaðarfyritøkur v.m. Vinnuhúsieth; - House of Industry; 2020.
[2] Umhvørvisstovan DES. Orkugoymslur í føroyum (Accessed 01-01-2021) URL, http://www.os.fo/media/1198/orkugoymsla-i-foeroyum-web.pdf.
[3] Trondheim HM, Niclasen BA, Nielsen T, Silva FFD, Bak CL. 100% sustainable electricity in the Faroe Islands: expansion planning through economic optimization. IEEE Open Access Journal of Power and Energy 2021;8:23–34. https://doi.org/10.1109/oajpe.2021.3051917.
[4] Katsaprakakis DA, Thomsen B, Dakanali I, Tzirakis K. Faroe Islands: towards 100% R.E.S. penetration. Renew Energy 2019;135:473–84. https://doi.org/10.1016/j.renene.2018.12.042.
[5] Aderinto T, Li H. ocean wave energy converters: status and challenges. Energies 2018;11(5):1250. https://doi.org/10.3390/en11051250.
[6] Kamranzad B, Takara K. A climate-dependent sustainability index for wave energy resources in Northeast Asia. Energy 2020;209:118466. https://doi.org/10.1016/j.energy.2020.118466.
[7] Karunarathna H, Maduwantha P, Kamranzad B, Rathnasooriya H, de Silva K. Evaluation of spatio-temporal variability of ocean wave power resource around Sri Lanka. Energy 2020;200:117503. https://doi.org/10.1016/j.energy.2020.117503.
[8] Kamranzad B, Lin P. Sustainability of wave energy resources in the South China Sea based on five decades of changing climate. Energy 2020;210:118604. https://doi.org/10.1016/j.energy.2020.118604.
[9] Ris RC, Holthuijsen LH, Booij N. A third-generation wave model for coastal regions: 2. verification. J Geophys Res: Oceans 1999;104(C4):7667–81. https://doi.org/10.1029/1998jc900123.
[10] Kobayashi S, Ota Y, Harada Y, Ebita A, Moriya M, Onoda H, Onogi K, Kamahori H, Kobayashi C, Endo H, Miyaoka K, Takahashi K. The JRA-55 reanalysis: General specifications and basic characteristics. Journal of the Meteorological Society of Japan. Ser. II 2015;93(1):5–48. https://doi.org/10.2151/jmsj.2015-001.
[11] Yang Z, Neary VS. High-resolution hindcasts for U.S. wave energy resource characterization. International Marine Energy Journal 2020;3(2):65–71. https://doi.org/10.36688/imej.3.65-71.
[12] Ahn S, Haas KA, Neary VS. Wave energy resource characterization and assessment for coastal waters of the United States. Appl Energy 2020;267:114922. https://doi.org/10.1016/j.apenergy.2020.114922.
[13] Ahn S, Neary VS. Non-stationary historical trends in wave energy climate for coastal waters of the United States. Ocean Eng 2020;216:108044. https://doi.org/10.1016/j.oceaneng.2020.108044.
[14] Allahdadi MN, Gunawan B, Lai J, He R, Neary VS. Development and validation of a regional-scale high-resolution unstructured model for wave energy resource characterization along the US East Coast. Renew Energy 2019;136:500–11. https://doi.org/10.1016/j.renene.2019.01.020.
[15] The WAVEWATCH III ® Development Group. User manual and system documentation of WAVEWATCH III ® version 5.16. pp. + Appendices. Tech. Note 329. NOAA/NWS/NCEP/MMAB; 2016. p. 326.
[16] Arinaga RA, Cheung KF. Atlas of global wave energy from 10 years of reanalysis and hindcast data. Renew Energy 2012;39(1):49–64. https://doi.org/10.1016/j.renene.2011.06.039.
[17] Iglesias G, Carballo R. Choosing the site for the first wave farm in a region: a case study in the Galician Southwest (Spain). Energy 2011;36(9):5525–31. https://doi.org/10.1016/j.energy.2011.07.022.
[18] Iglesias G, Carballo R. Wave resource in El Hierro—an island towards energy self-sufficiency. Renew Energy 2011;36(2):689–98. https://doi.org/10.1016/j.renene.2010.08.021.
[19] Iglesias G, López M, Carballo R, Castro A, Fraguela J, Frigaard P. Wave energy potential in Galicia (NW Spain). Renew Energy 2009;34(11):2323–33. https://doi.org/10.1016/j.renene.2009.03.030.

[20] The WAMDI Group. The WAM model—a third generation ocean wave prediction model. J Phys Oceanogr 1988;18(12):1775–810. https://doi.org/10.1175/1520-0485(1988)018<1775:TWMTGO>2.0.CO;2.
[21] Kalnay E, Kanamitsu M, Kistler R, Collins W, Deaven D, Gandin L, Iredell M, Saha S, White G, Woollen J, Zhu Y, Leetmaa A, Reynolds R, Chelliah M, Ebisuzaki W, Higgins W, Janowiak J, Mo KC, Ropelewski C, Wang J, Jenne R, Joseph D. The NCEP/NCAR 40-year reanalysis project. Bull Am Meteorol Soc 1996;77(3):437–71. https://doi.org/10.1175/1520-0477(1996)077<0437:tnyrp>2.0.co;2.
[22] Cats G, Wolters L. The hirlam project [meteorology]. IEEE Comput Sci Eng 1996;3(4):4–7. https://doi.org/10.1109/99.556505.
[23] Iglesias G, Carballo R. Wave energy potential along the death coast (Spain). Energy 2009;34(11):1963–75. https://doi.org/10.1016/j.energy.2009.08.004.
[24] Iglesias G, Carballo R. Offshore and inshore wave energy assessment: asturias (N Spain). Energy 2010;35(5):1964–72. https://doi.org/10.1016/j.energy.2010.01.011.
[25] Rusu E, Soares CG. Numerical modelling to estimate the spatial distribution of the wave energy in the Portuguese nearshore. Renew Energy 2009;34(6):1501–16. https://doi.org/10.1016/j.renene.2008.10.027.
[26] Iglesias G, Carballo R. Wave energy and nearshore hot spots: the case of the SE Bay of Biscay. Renew Energy 2010;35(11):2490–500. https://doi.org/10.1016/j.renene.2010.03.016.
[27] Venugopal V, Nemalidinne R. Wave resource assessment for Scottish waters using a large scale North Atlantic spectral wave model. Renew Energy 2015;76:503–25. https://doi.org/10.1016/j.renene.2014.11.056.
[28] DHI. MIKE 21 Spectral waves FM, user guide. Hørsholm, Denmark DHI, Agern Allé 2017;5:2970.
[29] ECMWF (Accessed 01-01-2021), https://cds.climate.copernicus.eu/.
[30] Rusu L, Soares CG. Wave energy assessments in the Azores islands. Renew Energy 2012;45:183–96. https://doi.org/10.1016/j.renene.2012.02.027.
[31] Rusu E, Soares CG. Wave energy pattern around the Madeira Islands. Energy 2012;45(1):771–85. https://doi.org/10.1016/j.energy.2012.07.013.
[32] Sierra J, González-Marco D, Sospedra J, Gironella X, Mösso C, Sánchez-Arcilla A. Wave energy resource assessment in Lanzarote (Spain). Renew Energy 2013;55:480–9. https://doi.org/10.1016/j.renene.2013.01.004.
[33] Gonçalves M, Martinho P, Soares CG. Assessment of wave energy in the canary islands. Renew Energy 2014;68:774–84. https://doi.org/10.1016/j.renene.2014.03.017.
[34] Rusu E, Onea F. Estimation of the wave energy conversion efficiency in the Atlantic Ocean close to the European islands. Renew Energy 2016;85:687–703. https://doi.org/10.1016/j.renene.2015.07.042.
[35] Davidsen E. Bølgeklimaet ved Fæøerne. Tech. rep. Polyteknisk læreanstalt; 1974.
[36] Etemad-Shahidi A, Kazeminezhad M, Mousavi S. On the prediction of wave parameters using simplified methods. Journal of Coastal Research (SPEC. ISSUE 2009;56:505–9.
[37] Guide to wave analysis and forecasting. Geneva, Switzerland: Secretariat of the World Meteorological Organization; 1998.
[38] Mühlestein D, Rugbjerg M. Wave atlas for the Faroe Islands. Tech. rep. DHI; 1998.
[39] Niclasen BA. An operation wave model for the Faroe Shelf. Ph.D. thesis. 2006.
[40] SeWave. Front end engineering design, tunneled wave energy converter for the Faroe Islands, tech. Rep. SeWave Ltd.; 2005.
[41] Niclasen B, Simonsen K. High resolution wave climate of the Faroe Islands. 2012.
[42] Ceverny R. 19-meter wave sets new record - highest significant wave height measured by a buoy (Accessed 01-01-2021), https://public.wmo.int/en/media/press-release/19-meter-wave-sets-new-record-highest-significant-wave-height-measured-buoy.
[43] DHI. MIKE 21 Wave modelling, spectral waves FM, short description. Hørsholm, Denmark DHI, Agern Allé 2017;5:2970.
[44] Komen GJ, Cavaleri L, Donelan M, Hasselmann K, Hasselmann S, Janssen PAEM. Dynamics and modelling of ocean waves. Cambridge University Press; 1994. https://doi.org/10.1017/cbo9780511628955.
[45] Janssen P. Wave induced stress and the drag of airflow over sea waves. J Phys Oceanogr 1989;19:745–54.
[46] Janssen P. Quasi-linear theory of wind wave generation applied to wave forecasting. J Phys Oceanogr 1991;19:1631–42.
[47] Hasselmann S, Hasselmann K, Allender J, Barnett T. Computations and parameterizations of the nonlinear energy transfer in a gravity wave spectrum. Part ii: parameterizations of the nonlinear transfer for application in wave models. J Phys Oceanogr 1985;15(11):1378–91.
[48] General bathymetric charts of the Oceans. GEBCO (Accessed 01-01-2021). URL, https://www.gebco.net/.
[49] Simonsen K, Larsen K, Mortensen L, Norbye A. New bathymetry for the Faroe Shelf, tech. Rep. University of the Faroe Islands; 2002.
[50] A. Wiese, J. Staneva, J. Schultz-Stellenfleth, A. Behrens, L. Fenoglio-Marc, J.-R. Bidlot, Synergy between satellite observations and model simulations during extreme eventsdoi:10.5194/os-2018-87.
[51] DHI. MIKE 21 spectral wave module. Scientific documentation; 2017.
[52] Nortek. Wave systems - AWAC (Accessed 01-01-2021). URL, http://195.62.126.26/en/products/wave-systems/awac.
[53] Davidsen E, Hansen B. The Faroese wave- and current-measuring project. Coast Eng 1981;5:111–23. https://doi.org/10.1016/0378-3839(81)90010-7.
[54] Niclasen B, Simonsen K. Note on wave parameters from moored wave buoys. Appl Ocean Res 2007;29(4):231–8. https://doi.org/10.1016/j.apor.2008.01.003.
[55] Landsverk. Webpage (Accessed 01-01-2021). URL, https://www.landsverk.fo.